ε	Dielectric constant
η	Overvoltage
μ	Ionic strength
ν	Kinematic viscosity
ω	Angular velocity

1

FUNDAMENTAL CONCEPTS

1.1 WHY ELECTROANALYSIS?

Electroanalytical techniques are concerned with the interplay between electricity and chemistry, namely, the measurements of electrical quantities, such as current, potential, or charge and their relationship to chemical parameters. Such use of electrical measurements for analytical purposes has found a vast range of applications, including environmental monitoring, industrial quality control, or biomedical analysis. Advances since the mid-1980s, including the development of ultramicroelectrodes, the design of tailored interfaces and molecular monolayers, the coupling of biological components and electrochemical transducers, the synthesis of ionophores and receptors containing cavities of molecular size, the development of ultratrace voltammetric techniques or of high-resolution scanning probe microscopies, and the microfabrication of molecular devices or efficient flow detectors, have led to a substantial increase in the popularity of electroanalysis and to its expansion into new phases and environments. Indeed, electrochemical probes are receiving a major share of the attention in the development of chemical sensors.

In contrast to many chemical measurements, which involve homogeneous bulk solutions, electrochemical processes take place at the electrode–solution interface. The distinction between various electroanalytical techniques reflects the type of electrical signal used for the quantitation. The two principal types

Analytical Electrochemistry, Third Edition, by Joseph Wang
Copyright © 2006 John Wiley & Sons, Inc.

of electroanalytical measurements are potentiometric and potentiostatic. Both types require at least two electrodes (conductors) and a contacting sample (electrolyte) solution, which constitute the electrochemical cell. The electrode surface is thus a junction between an ionic conductor and an electronic conductor. One of the two electrodes responds to the target analyte(s) and is thus termed the *indicator* (or *working*) electrode. The second one, termed the *reference* electrode, is of constant potential (i.e., independent of the properties of the solution). Electrochemical cells can be classified as *electrolytic* (when they consume electricity from an external source) or *galvanic* (if they are used to produce electrical energy).

Potentiometry (discussed in Chapter 5), which is of great practical importance, is a static (zero-current) technique in which the information about the sample composition is obtained from measurement of the potential established across a membrane. Different types of membrane materials, possessing different ion recognition processes, have been developed to impart high selectivity. The resulting potentiometric probes have thus been widely used for several decades for direct monitoring of ionic species such as protons or calcium, fluoride, and potassium ions in complex samples.

Controlled-potential (potentiostatic) techniques deal with the study of charge transfer processes at the electrode–solution interface, and are based on dynamic (non-zero-current) situations. Here, the electrode potential is being used to derive an electron transfer reaction and the resultant current is measured. The role of the potential is analogous to that of the wavelength in optical measurements. Such a controllable parameter can be viewed as "electron pressure," which forces the chemical species to gain or lose an electron (reduction or oxidation, respectively). Accordingly, the resulting current reflects the rate at which electrons move across the electrode–solution interface. Potentiostatic techniques can thus measure any chemical species that is electroactive, that is, that can be made to reduce or oxidize. Knowledge of the reactivity of functional group in a given compound can be used to predict its electroactivity. Nonelectroactive compounds may also be detected in connection with indirect or derivatization procedures.

The advantages of controlled-potential techniques include high sensitivity, selectivity toward electroactive species, a wide linear range, portable and low-cost instrumentation, speciation capability, and a wide range of electrodes that allow assays of unusual environments. Several properties of these techniques are summarized in Table 1.1. Extremely low (nanomolar) detection limits can be achieved with very small (5–20-μL) sample volumes, thus allowing the determination of analyte amounts ranging from 10^{-13} to 10^{-15} mol on a routine basis. Improved selectivity may be achieved via the coupling of controlled-potential schemes with chromatographic or optical procedures.

This chapter attempts to give an overview of electrode processes, together with discussion of electron transfer kinetics, mass transport, and the electrode–solution interface.

TABLE 1.1 Properties of Controlled-Potential Techniques[a]

Technique	Working Electrode	Detection Limit (M)	Speed (Time per Cycle) (min)	Response Shape
DC polarography	DME	10^{-5}	3	Wave
NP polarography	DME	5×10^{-7}	3	Wave
DP polarography	DME	10^{-8}	3	Peak
DP voltammetry	Solid	5×10^{-7}	3	Peak
SW polarography	DME	10^{-8}	0.1	Peak
AC polarography	DME	5×10^{-7}	1	Peak
Chronoamperometry	Stationary	10^{-5}	0.1	Transient
Cyclic voltammetry	Stationary	10^{-5}	0.1–2	Peak
Stripping voltammetry	HMDE, MFE	10^{-10}	3–6	Peak
Adsorptive stripping voltammetry	HMDE	10^{-10}	2–5	Peak
Adsorptive stripping voltammetry	Solid	10^{-9}	4–5	Peak
Adsorptive catalytic stripping voltammetry	HMDE	10^{-12}	2–5	Peak

[a] All acronyms used here are included in the "Abbreviations and Symbols" list following the Preface.

1.2 FARADAIC PROCESSES

The objective of controlled-potential electroanalytical experiments is to obtain a current response that is related to the concentration of the target analyte. Such an objective is accomplished by monitoring the transfer of electron(s) during the redox process of the analyte:

$$O + ne^- \rightleftharpoons R \tag{1.1}$$

where O and R are the oxidized and reduced forms, respectively, of the redox couple. Such a reaction will occur in a potential region that makes the electron transfer thermodynamically or kinetically favorable. For systems controlled by the laws of thermodynamics, the potential of the electrode can be used to establish the concentration of the electroactive species at the surface [$C_O(0,t)$ and $C_R(0,t)$] according to the Nernst equation

$$E = E^\circ + \frac{2.3RT}{nF} \log \frac{C_O(0,t)}{C_R(0,t)} \tag{1.2}$$

where E° is the standard potential for the redox reaction, R is the universal gas constant ($8.314\,J\,K^{-1}\,mol^{-1}$), T is the Kelvin temperature, n is the number of electrons transferred in the reaction, and F is the Faraday constant [96,487 C

(coulombs)]. On the negative side of $E°$, the oxidized form thus tends to be reduced, and the forward reaction (i.e., reduction) is more favorable. The current resulting from a change in oxidation state of the electroactive species is termed the *faradaic current* because it obeys Faraday's law (i.e., the reaction of 1 mol of substance involves a change of $n \times 96{,}487$ C). The faradaic current is a direct measure of the rate of the redox reaction. The resulting current–potential plot, known as the *voltammogram*, is a display of current signal [vertical axis (ordinate)] versus the excitation potential [horizontal axis (abscissa)]. The exact shape and magnitude of the voltammetric response is governed by the processes involved in the electrode reaction. The total current is the summation of the faradaic currents for the sample and blank solutions, as well as the nonfaradaic charging background current (discussed in Section 1.3).

The pathway of the electrode reaction can be quite complicated, and takes place in a sequence that involves several steps. The rate of such reactions is determined by the slowest step in the sequence. Simple reactions involve only mass transport of the electroactive species to the electrode surface, electron transfer across the interface, and transport of the product back to the bulk solution. More complex reactions include additional chemical and surface processes that either precede or follow the actual electron transfer. The net rate of the reaction, and hence the measured current, may be limited by either mass transport of the reactant or the rate of electron transfer. The more sluggish process will be the rate-determining step. Whether a given reaction is controlled by mass transport or electron transfer is usually determined by the type of compound being measured and by various experimental conditions (electrode material, media, operating potential, mode of mass transport, time scale, etc.). For a given system, the rate-determining step may thus depend on the potential range under investigation. When the overall reaction is controlled solely by the rate at which the electroactive species reach the surface (i.e., a facile electron transfer), the current is said to be *mass-transport-limited*. Such reactions are called *nernstian* or *reversible*, because they obey thermodynamic relationships. Several important techniques (discussed in Chapter 4) rely on such mass-transport-limited conditions.

1.2.1 Mass-Transport-Controlled Reactions

Mass transport occurs by three different modes:

- *Diffusion*—the spontaneous movement under the influence of concentration gradient, from regions of high concentrations to regions of lower ones, aimed at minimizing concentration differences.
- *Convection*—transport to the electrode by a gross physical movement; the major driving force for convection is an external mechanical energy associated with stirring or flowing the solution or rotating or vibrating the electrode (i.e., forced convection). Convection can also occur naturally as a result of density gradients.
- *Migration*—movement of charged particles along an electrical field (i.e., where the charge is carried through the solution by ions according to their transference number).

These modes of mass transport are illustrated in Figure 1.1.

The *flux* (J), a common measure of the rate of mass transport at a fixed point, is defined as the number of molecules penetrating a unit area of an imaginary plane in a unit of time and is expressed in units of mol cm^{-2} s^{-1}. The flux to the electrode is described mathematically by a differential equation, known as the *Nernst–Planck equation*, given here for one dimension

$$J(x,t) = -D\frac{\partial C(x,t)}{\partial x} - \frac{zFDC}{RT}\frac{\partial \phi(x,t)}{\partial x} + C(x,t)V(x,t) \qquad (1.3)$$

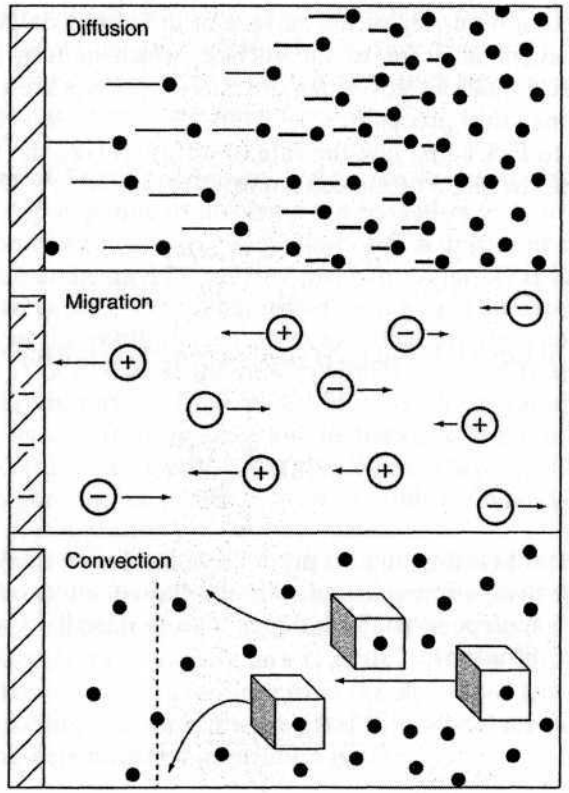

Figure 1.1 The three modes of mass transport. (Reproduced with permission from Ref. 1.)

where D is the diffusion coefficient (cm^2/s); $[\partial C(x,t)]/\partial x$ is the concentration gradient (at distance x and time t); $[\partial \phi(x,t)]/\partial x$ is the potential gradient; z and C are the charge and concentration, respectively, of the electroactive species; and $V(x,t)$ is the hydrodynamic velocity (in the x direction). In aqueous media, D usually ranges between 10^{-5} and 10^{-6} cm^2/s. The current (i) is directly proportional to the flux and the surface area (A):

$$i = -nFAJ \tag{1.4}$$

As indicated by Eq. (1.3), the situation is quite complex when the three modes of mass transport occur simultaneously. This complication makes it difficult to relate the current to the analyte concentration. The situation can be greatly simplified by suppressing the electromigration through the addition of excess inert salt. This addition of a high concentration of the supporting electrolyte (compared to the concentration of electroactive ions) helps reduce the electrical field by increasing the solution conductivity. Convection effects can be eliminated by using a quiescent solution. In the absence of migration and convection effects, movement of the electroactive species is limited by diffusion. The reaction occurring at the surface of the electrode generates a concentration gradient adjacent to the surface, which in turn gives rise to a diffusional flux. Equations governing diffusion processes are thus relevant to many electroanalytical procedures.

According to Fick's first law, the rate of diffusion (i.e., the flux) is directly proportional to the slope of the concentration gradient:

$$J(x,t) = -D\frac{\partial C(x,t)}{\partial x} \tag{1.5}$$

Combination of Eqs. (1.4) and (1.5) yields a general expression for the current response:

$$i = nFAD\frac{\partial C(x,t)}{\partial x} \tag{1.6}$$

Hence, the current (at any time) is proportional to the concentration gradient of the electroactive species. As indicated by the equations above, the diffusional flux is time-dependent. Such dependence is described by Fick's second law (for linear diffusion):

$$\frac{\partial C(x,t)}{\partial t} = D\frac{\partial^2 C(x,t)}{\partial x^2} \tag{1.7}$$

This equation reflects the rate of change with time of the concentration between parallel planes at points x and $(x + dx)$ (which is equal to the difference in flux at the two planes). Fick's second law is valid for the conditions assumed, namely, planes parallel to one another and perpendicular to the direction of diffusion, specifically, conditions of linear diffusion. In contrast, for the case of diffusion toward a spherical electrode (where the lines of flux are not parallel but are perpendicular to segments of the sphere), Fick's second law is expressed as

$$\frac{\partial C}{\partial t} = D\left[\frac{\partial^2 C}{\partial r^2} + \frac{2}{r}\frac{\partial C}{\partial r}\right] \tag{1.8}$$

where r is the distance from the center of the electrode. Overall, Fick's laws describe the flux and the concentration of the electroactive species as functions of position and time. The solution of these partial differential equations usually requires application of a (Laplace transformation) mathematical method. The Laplace transformation is of great value for such application, as it enables the conversion of the problem into a domain where a simpler mathematical manipulation is possible. Details of using the Laplace transformation are beyond the scope of this text, and can be found in Ref. 2. The establishment of proper initial and boundary conditions (which depend on the specific experiment) is also essential for this treatment. The current–concentration–time relationships resulting from such treatment are described below for several relevant experiments.

1.2.1.1 Potential-Step Experiment Let us see, for example, what happens in a potential-step experiment involving the reduction of O to R, a potential value corresponding to complete reduction of O, a quiescent solution, and a planar electrode embedded in a planar insulator. (Only O is initially present in solution.) The current–time relationship during such an experiment can be understood from the resulting concentration–time profiles. Since the surface concentration of O is zero at the new potential, a concentration gradient is established near the surface. The region within which the solution is depleted of O is known as the *diffusion layer*, and its thickness is given by δ. The concentration gradient is steep at first, and the diffusion layer is thin (see Fig. 1.2 for t_1). As time goes by, the diffusion layer expands (to δ_2 and δ_3 at t_2 and t_3), and hence the concentration gradient decreases.

Initial and boundary conditions in such an experiment include $C_O(x,0) = C_O(b)$ [i.e., at $t = 0$, the concentration is uniform throughout the system and equal to the bulk concentration, $C_O(b)$], $C_O(0,t) = 0$ for $t > 0$ (i.e., at later times the surface concentration is zero); and $C_O(x,0) \rightarrow C_O(b)$ as $x \rightarrow \infty$ (i.e., the concentration increases as the distance from the electrode increases). Solution to Fick's laws (for linear diffusion, i.e., a planar electrode) for these conditions results in a time-dependent concentration profile:

$$C_O(x,t) = C_O(b)\left\{1 - \mathrm{erf}\left[x/(4D_O t)^{1/2}\right]\right\} \tag{1.9}$$

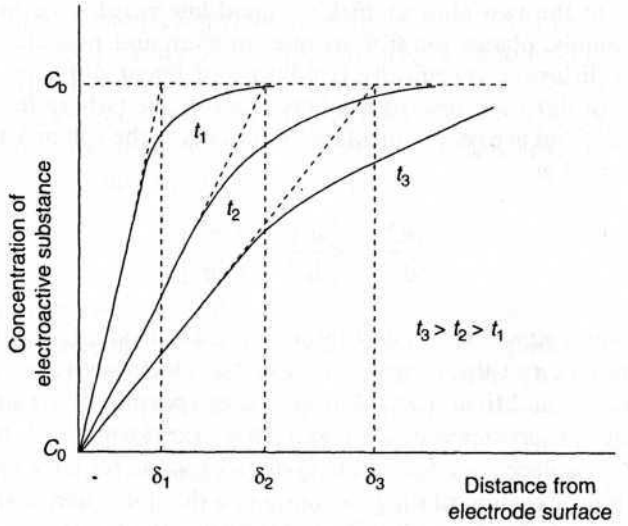

Figure 1.2 Concentration profiles for different times after the start of a potential-step experiment.

whose derivative with respect to x gives the concentration gradient at the surface

$$\frac{\partial C}{\partial x} = C_O(b)/(\pi D_O t)^{1/2} \tag{1.10}$$

when substituted into Eq. (1.6) leads to the well-known *Cottrell equation*:

$$i(t) = nFAD_O C_O(b)/(\pi D_O t)^{1/2} \tag{1.11}$$

Thus, the current decreases in proportion to the square root of time, with $(\pi D_O t)^{1/2}$ corresponding to the diffusion-layer thickness.

Solving Eq. (1.8) (using Laplace transform techniques) will yield the time evolution of the current of a spherical electrode:

$$i(t) = nFAD_O C_O(b)/(\pi D_O t)^{1/2} + nFAD_O C_O/r \tag{1.12}$$

The current response of a spherical electrode following a potential step thus contains both time-dependent and time-independent terms—reflecting the planar and spherical diffusional fields, respectively (Fig. 1.3)—becoming time independent at long timescales. As expected from Eq. (1.12), the change from one regime to another is strongly dependent on the radius of the electrode.

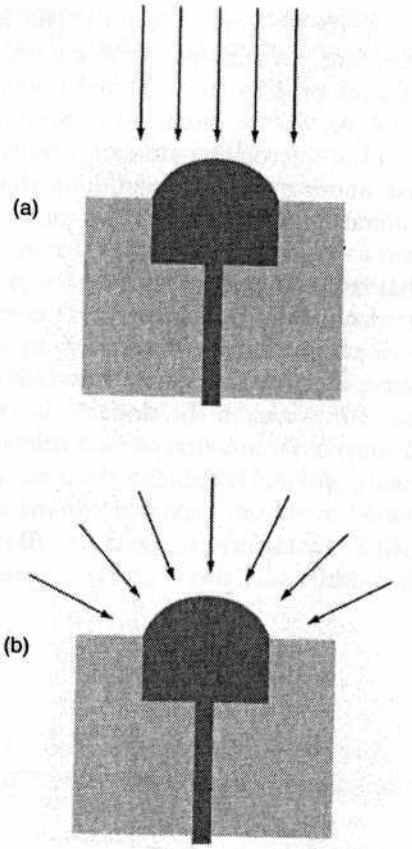

Figure 1.3 Planar (a) and spherical (b) diffusional fields at spherical electrodes.

The unique mass transport properties of ultramicroelectrodes (discussed in Section 4.5.4) are attributed to shrinkage of the electrode radius.

1.2.1.2 Potential-Sweep Experiments Let us move to a voltammetric experiment involving a linear potential scan, the reduction of O to R and a quiescent solution. The slope of the concentration gradient is given by $(C_O(b,t) - C_O(0,t))/\delta$, where $C_O(b,t)$ and $C_O(0,t)$ are the bulk and surface concentrations of O. The change in the slope, and hence the resulting current, are due to changes of both $C_O(0,t)$ and δ. First, as the potential is scanned negatively, and approaches the standard potential ($E°$) of the couple, the surface concentration rapidly decreases in accordance with the Nernst equation [Eq. (1.2)]. For example, at a potential equal to $E°$ the concentration ratio is unity $[C_O(0,t)/C_R(0,t) = 1]$. For a potential 59 mV more negative than $E°$, $C_R(0,t)$ is present at 10-fold excess $[C_O(0,t)/C_R(0,t)] = 1/10 (n = 1)$. The decrease in $C_O(0,t)$ is coupled with an increase in the diffusion-layer thickness, which dominates the

change in slope after $C_O(0,t)$ approaches zero. The net result is a peak-shaped voltammogram. Such current–potential curves and the corresponding concentration–distance profiles (for selected potentials along the scan) are shown in Figure 1.4. As will be discussed in Section 4.5.4, shrinking the electrode dimension to the micrometer domain results in a sigmoid-shaped voltammetric response under quiescent conditions, characteristic of the different (radial) diffusional field and higher flux of electroactive species of ultramicroelectrodes.

Let us see now what happens in a similar linear scan voltammetric experiment, but utilizing a stirred solution. Under these conditions, the bulk concentration ($C_{O(b,t)}$) is maintained at a distance δ by the stirring. It is not influenced by the surface electron transfer reaction (as long as the electrode-area : solution-volume ratio is small). The slope of the concentration–distance profile $\{[C_O(b,t) - C_O(0,t)]/\delta\}$ is thus determined solely by the change in the surface concentration $[C_O(0,t)]$. Hence, the decrease in $C_O(0,t)$ during the potential scan (around E°) results in a sharp rise in the current. When a potential more negative than E° by 118 mV is reached, $C_O(0,t)$ approaches zero, and a limiting current (i_l) is achieved:

$$i_l = \frac{nFAD_OC_O(b,t)}{\delta} \tag{1.13}$$

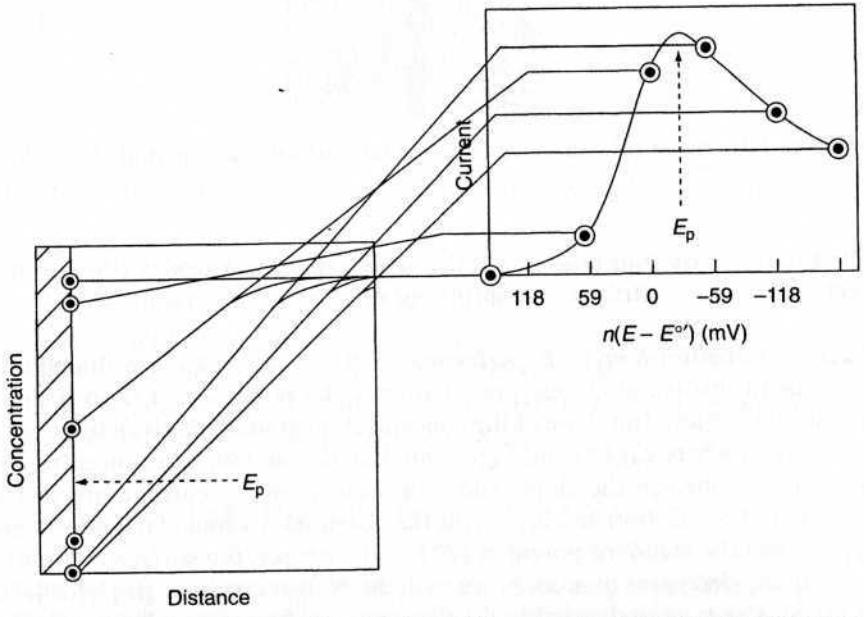

Figure 1.4 Concentration profiles (left) for different potentials during a linear sweep voltammetric experiment in unstirred solution. The resulting voltammogram is shown on the right, along with the points corresponding to each concentration gradient. (Reproduced with permission from Ref. 1.)

The resulting voltammogram thus has a sigmoidal (wave) shape. By increasing the stirring rate (U), the diffusion layer thickness becomes thinner, according to

$$\delta = \frac{B}{U^\alpha} \tag{1.14}$$

where B and α are constants for a given system. As a result, the concentration gradient becomes steeper (see Fig. 1.5, curve *b*), thereby increasing the limiting current. Similar considerations apply to other forced convection systems, including those relying on solution flow or electrode rotation (see Sections 3.6 and 4.5, respectively). For all of these hydrodynamic systems, the sensitivity of the measurement can be enhanced by increasing the convection rate.

Initially it was assumed that no solution movement occurs within the diffusion layer. Actually, a velocity gradient exists in a layer, termed the *hydrodynamic boundary layer* (or the *Prandtl layer*), where the fluid velocity increases from zero at the interface to the constant bulk value (U). The thickness of the hydrodynamic layer δ_H is related to that of the diffusion layer

$$\delta \cong \left(\frac{D}{\nu}\right)^{1/3} \delta_H \tag{1.15}$$

where ν is kinematic viscosity. In aqueous media (with $\nu \sim 10^{-2}$ cm^2/s and $D \sim 10^{-5}$ cm^2/s), δ_H is approximately 10-fold larger than δ, indicating negligible con-

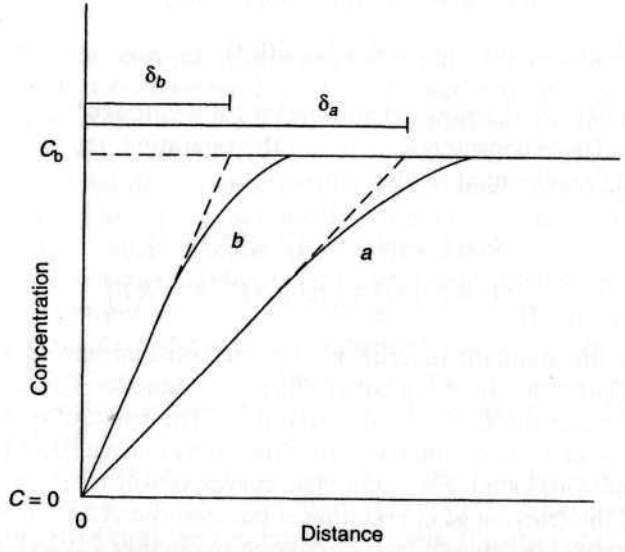

Figure 1.5 Concentration profiles for two rates of convection transport: low (curve *a*) and high (curve *b*).

vection within the diffusion layer. The discussion above applies to other forced convection systems, such as flow detectors or rotating electrodes (see Sections 3.6 and 4.5, respectively). Layer thickness (δ) values of 10–50 μm and 100–150 μm are common for electrode rotation and solution stirring, respectively. Additional means for enhancing the mass transport and thinning the diffusion layer, including the use of power ultrasound, heated electrodes, or laser activation, are also being studied (3,4). These methods may simultaneously minimize surface fouling effects, as desired for retaining the surface reactivity.

1.2.2 Reactions Controlled by the Rate of Electron Transfer

In this section we consider experiments in which the current is controlled by the rate of electron transfer (i.e., reactions with sufficiently fast mass transport). The current–potential relationship for such reactions is different from those discussed (above) for mass-transport-controlled reactions.

Consider again the electron transfer reaction: $O + ne^- \rightleftharpoons R$; the actual electron transfer step involves transfer of the electron between the conduction band of the electrode and a molecular orbital of O or R (e.g., for a reduction, from the conduction band into an unoccupied orbital in O). The rate of the forward (reduction) reaction V_f is first-order in O:

$$V_f = k_f C_O(0,t) \tag{1.16}$$

while that of the reversed (oxidation) reaction V_b, is first-order in R:

$$V_b = k_b C_R(0,t) \tag{1.17}$$

where k_f and k_b are the forward and backward heterogeneous rate constants, respectively. These constants depend on the operating potential according to the following exponential relationships:

$$k_f = k^\circ \exp[-\alpha n F(E - E^\circ)/RT] \tag{1.18}$$

$$k_b = k^\circ \exp[(1-\alpha) n F(E - E^\circ)/RT] \tag{1.19}$$

where k° is the standard heterogeneous rate constant and α is the transfer coefficient. The value of k° (in cm/s) reflects the reaction between the particular reactant and the electrode material used. The value of α (between zero and unity) reflects the symmetry of the free-energy curve (with respect to the reactants and products). For symmetric curves, α will be close to 0.5; α is a measure of the fraction of energy that is put into the system used to actually lower the activation energy (see discussion in Section 1.2.2.1). Overall, Eqs. (1.18) and (1.19) indicate that by changing the applied potential, we influence k_f and k_b in an exponential fashion. Positive and negative potentials thus speed

up the oxidation and reduction reactions, respectively. For an oxidation, the energy of the electrons in the donor orbital of R must be equal to or higher than the energy of electrons in the electrode. For reduction, the energy of the electrons in the electrode must be higher than their energy in the receptor orbital of R.

Since the net reaction rate is

$$V_{net} = V_f - V_b = k_f C_O(0,t) - k_b C_R(0,t) \tag{1.20}$$

and as the forward and backward currents are proportional to V_f and V_b, respectively

$$i_f = nFAV_f \tag{1.21}$$

$$i_b = nFAV_b \tag{1.22}$$

the overall current is given by the difference between the currents due to the forward and backward reactions:

$$i_{net} = i_f - i_b = nFA[k_f C_O(0,t) - k_b C_R(0,t)] \tag{1.23}$$

By substituting the expressions for k_f and k_b [Eqs. (1.17) and (1.18), respectively], one obtains the *Butler–Volmer equation*:

$$i = nFAk^\circ\{C_O(0,t)\exp[-\alpha n F(E - E^\circ)/RT] - C_R(0,t)\exp[(1-\alpha) n F(E - E^\circ)/RT]\} \tag{1.24}$$

which describes the current–potential relationship for reactions controlled by the rate of electron transfer. Note that the net current depends on both the operating potential and the surface concentration of each form of the redox (reduction–oxidation) couple. For example, Figure 1.6 displays the current–potential dependence for the case where $C_O(0,t) = C_R(0,t)$ and $\alpha = 0.50$. Large negative potentials accelerate the movement of charge in the cathodic direction, and also decelerate the charge movement in the opposite direction. As a result, the anodic current component becomes negligible and the net current merges with the cathodic component. The acceleration and deceleration of the cathodic and anodic currents are not necessarily as symmetric (as depicted in Fig. 1.6), and would differ for α values different from 0.5. Similarly, no cathodic current contribution is observed at sufficiently large positive potentials.

When $E = E^\circ$, no net current is flowing. This situation, however, is dynamic with continuous movement of charge carriers in both directions and with equal opposing anodic and cathodic current components. The absolute magnitude of these components at E° is the *exchange current* (i_0), which is directly proportional to the standard rate constant:

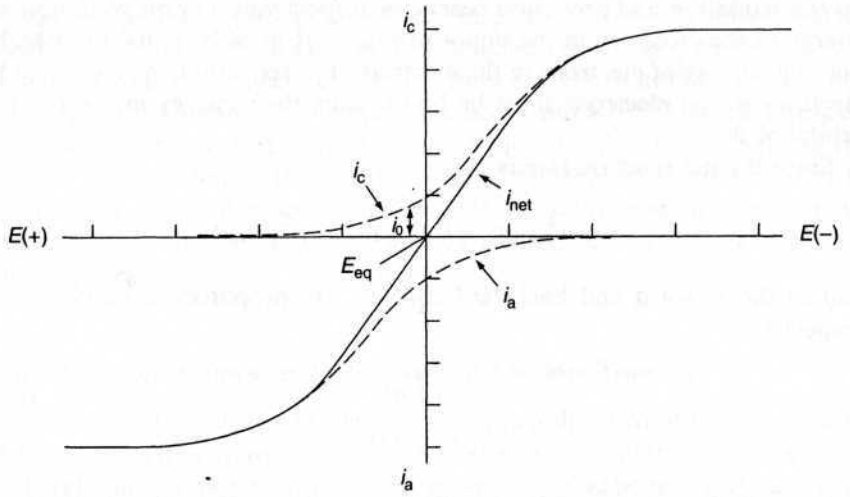

Figure 1.6 Current–potential curve for the system O + ne ↔ R, assuming that electron transfer is rate-limiting, $C_0 = C_R$, and $\alpha = 0.5$. The dotted lines show the i_c and i_a components.

$$i_0 = i_c = i_a = nFAk°C \tag{1.25}$$

The exchange current density for common redox couples (at room temperature) can range from 10^{-6} μA/cm^2 to A/cm^2. The Butler–Volmer equation can be written in terms of the exchange current

$$i = i_0[\exp(-\alpha nF\eta/RT) - \exp((1-\alpha)nF\eta/RT)] \tag{1.26}$$

where $\eta = E - E_{eq}$ is the *overvoltage* (i.e., the extra potential beyond the equilibration potential leading to a net current i). The overvoltage is always defined with respect to a specific reaction, for which the equilibrium potential is known.

Equation (1.26) can be used for extracting information on i_0 and α, which are important kinetic parameters. For sufficiently large overvoltages ($\eta >$ 118mV/n), one of the exponential terms in Eq. (1.26) will be negligible compared with the other. For example, at large negative overpotentials, $i_c \gg i_a$ and Eq. (1.26) becomes

$$i = i_0 \exp(-\alpha nF\eta/RT) \tag{1.27}$$

and hence, we get

$$\ln i = \ln i_0 - \alpha nF\eta/RT \tag{1.28}$$

This logarithmic current–potential dependence was derived by Tafel, and is known as the *Tafel equation*. By plotting log i against η one obtains the Tafel plots for the cathodic and anodic branches of the current–overvoltage curve (Fig. 1.7). Such plots are linear only at high overpotential values; severe deviations from linearity are observed as η approaches zero. Extrapolation of the linear portions of these plots to the zero overvoltage gives an intercept, which corresponds to log i_0; the slope can be used to obtain the value of the transfer coefficient α. Another form of the Tafel equation is obtained by rearrangement of Eq. (1.28):

$$\eta = a - b\log i \tag{1.29}$$

with b, the Tafel slope, having the value of $2.303RT/\alpha nF$. For $\alpha = 0.5$ and $n =$ 1, this corresponds to 118mV (at 25°C). Equation (1.29) indicates that the application of small potentials (beyond the equilibrium potential) can increase the current by many orders of magnitude. In practice, however, the current could not rise to an infinite value because of restrictions imposed by the rate at which the reactant reaches the surface. (Recall that the rate-determining step depends on the potential region.)

For small departures from $E°$, the exponential term in Eq. (1.27) may be linearized, with the current approximately proportional to η:

$$i = i_0 nF\eta/RT \tag{1.30}$$

Hence, the net current is directly proportional to the overvoltage in a narrow potential range near $E°$.

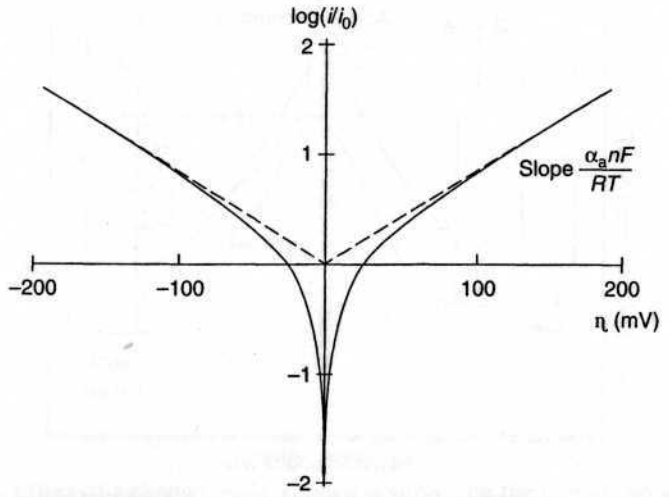

Figure 1.7 Tafel plots for cathodic and anodic branches of the current–potential curve.

Note also that at equilibrium ($E = E_{eq}$) the net current is zero (i.e., equal currents are passing reversibly in both directions); one can thus obtain the following from Eq. (1.24):

$$C_O(0,t)\exp[-\alpha nF(E-E^\circ)/RT] = C_R(0,t)\exp[(1-\alpha)nF(E-E^\circ)/RT] \quad (1.31)$$

Rearrangement of Eq. (1.31) yields the exponential form of the Nernst equation

$$\frac{C_O(0,t)}{C_R(0,t)} = \exp[nF(E-E^\circ)/RT] \quad (1.32)$$

expected for equilibrium conditions.

The equilibrium potential for a given reaction is related to the formal potential

$$E_{eq} = E^\circ + (2.3RT/nF)\log Q \quad (1.33)$$

where Q is the equilibrium ratio function (i.e., ratio of the equilibrium concentrations).

1.2.2.1 Activated Complex Theory The effect of the operating potential on the rate constants [Eqs. (1.18) and (1.19)] can be understood in terms of the free-energy barrier. Figure 1.8 shows a typical Morse potential energy

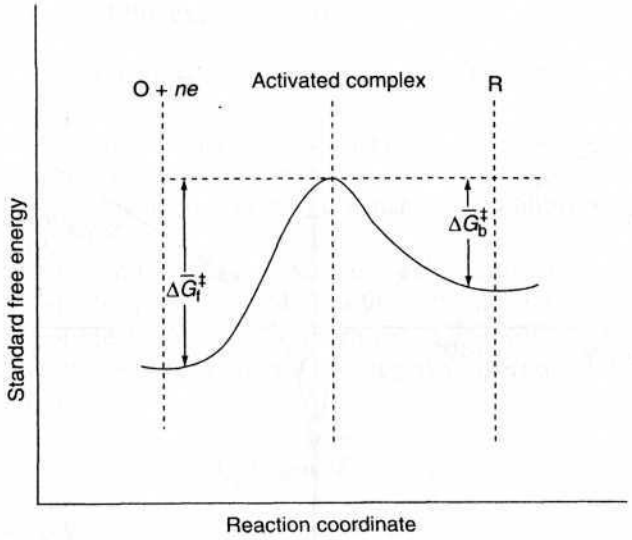

Figure 1.8 Free-energy curve for a redox process at a potential more positive than the equilibrium value.

curve for the reaction $O + ne^- \rightleftharpoons R$, at an inert metallic electrode (where O and R are soluble). Because of the somewhat different structures of O and R, there is a barrier to electron transfer (associated with changes in bond lengths and bond angles). In order for the transition from the oxidized form to occur, it is thus necessary to overcome the free energy of activation, $\Delta G^\ddagger$. The frequency with which the electron crosses the energy barrier as it moves from the electrode to O (i.e., the rate constant) is given by

$$k = Ae^{-\Delta G^\ddagger/RT} \quad (1.34)$$

Any alteration in $\Delta G^\ddagger$ will thus affect the rate of the reaction. If $\Delta G^\ddagger$ is increased, the reaction rate will decrease. At equilibrium, the cathodic and anodic activation energies are equal ($\Delta G^\ddagger_{c,0} = \Delta G^\ddagger_{a,0}$) and the probability of electron transfer will be the same in both directions. A, known as the frequency factor, is given as a simple function of the Boltzmann constant k' and the Planck constant, h:

$$A = \frac{k'T}{h} \quad (1.35)$$

Now let us discuss nonequilibirum situations. By varying the potential of the working electrode, we can influence the free energy of its resident electrons, thus making one reaction more favorable. For example, a potential shift E from the equilibrium value moves the $O + ne^-$ curve up or down by $\phi = -nFE$. The dashed line in Figure 1.9 displays such a change for the case of

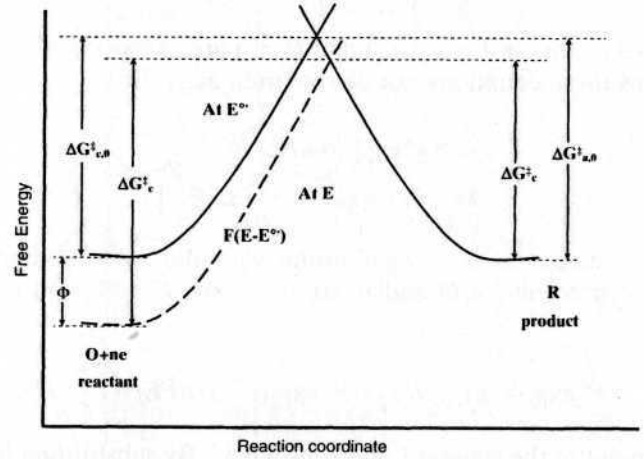

Figure 1.9 Effect of a change in the applied potential on the free energies of activation for reduction and oxidation.

a positive E. Under this condition the barrier for reduction, $\Delta G_c^{\ddagger}$, is larger than $\Delta G_{c,0}^{\ddagger}$. A careful study of the new curve reveals that only a fraction (α) of the energy shift ϕ is actually used to increase the activation energy barrier, and hence to accelerate the rate of the reaction. On the basis of the symmetry of the two potential curves, this fraction (the transfer coefficient) can range from zero to unity. Measured values of α in aqueous solutions have ranged from 0.2 to 0.8. The term α is thus a measure of the symmetry of the activation energy barrier. A α value of 0.5 indicates that the activated complex is exactly halfway between the reagents and products on the reaction coordinate (i.e., an idealized curve); α values close to 0.5 are common for metallic electrodes with a simple electron transfer process. The barrier for reduction at E is thus given by

$$\Delta G_c^{\ddagger} = \Delta G_{c,0}^{\ddagger} + \alpha nFE \tag{1.36}$$

Similarly, examination of the figure reveals also that the new barrier for oxidation, $\Delta G_a^{\ddagger}$, is lower than $\Delta G_{a,0}^{\ddagger}$:

$$\Delta G_a^{\ddagger} = \Delta G_{a,0}^{\ddagger} - (1-\alpha)nFE \tag{1.37}$$

By substituting the expressions for $\Delta G^{\ddagger}$ [Eqs. (1.36) and (1.37)] in Eq. (1.34), we obtain the following equations for reduction

$$k_f = A\exp[-\Delta G_{c,0}^{\ddagger}/RT]\cdot\exp[-\alpha nFE/RT] \tag{1.38}$$

and for oxidation:

$$k_b = A\exp[-\Delta G_{a,0}^{\ddagger}/RT]\cdot\exp[(1-\alpha)nFE/RT] \tag{1.39}$$

The first two factors in Eqs. (1.38) and (1.39) are independent of the potential, and thus these equations can be rewritten as

$$k_f = k_f^{\circ}\exp[-\alpha nFE/RT] \tag{1.40}$$

$$k_b = k_b^{\circ}\exp[(1-\alpha)nFE/RT] \tag{1.41}$$

When the electrode is at equilibrium with the solution, and when the surface concentrations of O and R are the same, $E = E^{\circ}$, and k_f and k_b are equal

$$k_f^{\circ}\exp[-\alpha nFE/RT] = k_b^{\circ}\exp[(1-\alpha)nFE/RT] = k^{\circ} \tag{1.42}$$

and correspond to the standard rate constant k°. By substituting for k_f° and k_b° [using Eq. (1.42)] in Eqs. (1.40) and (1.41), one obtains Eqs. (1.18) and (1.19) (which describe the effect of the operating potential on the rate constants).

1.3 ELECTRICAL DOUBLE LAYER

The electrical double layer is the array of charged particles and/or oriented dipoles existing at every material interface. In electrochemistry, such a layer reflects the ionic zones formed in the solution, to compensate for the excess of charge on the electrode (q_e). A positively charged electrode thus attracts a layer of negative ions (and vice versa). Since the interface must be neutral, $q_e + q_s = 0$ (where q_s is the charge of the ions in the nearby solution). Accordingly, such a counterlayer consists of ions of sign opposite that of the electrode. As illustrated in Figure 1.10, the electrical double layer has a complex structure of several distinct parts.

The inner layer (closest to the electrode), known as the *inner Helmholz plane* (IHP), contains solvent molecules and specifically adsorbed ions (such as Br^- or I^- that are not hydrated in aqueous solutions). It is defined by the locus of points for the specifically adsorbed ions. The next layer, the *outer Helmholz plane* (OHP), reflects the imaginary plane passing through the

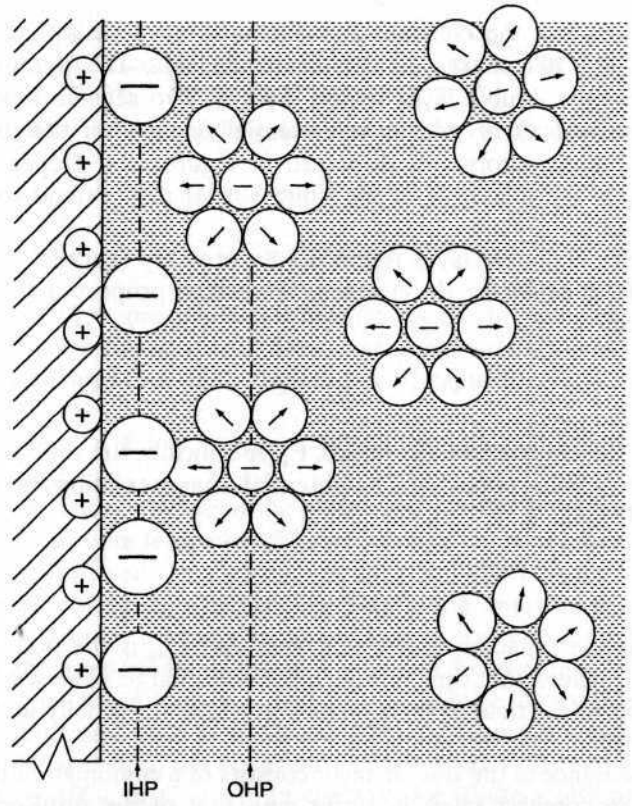

Figure 1.10 Schematic representation of the electrical double layer.

center of solvated ions at their closest approach to the surface. The solvated ions are nonspecifically adsorbed and are attracted to the surface by long-range coulombic forces. Both Helmholz layers represent the compact layer. Such a compact layer of charges is strongly held by the electrode and can survive even when the electrode is pulled out of the solution. The Helmholz model does not take into account the thermal motion of ions, which loosens them from the compact layer.

The outer layer (beyond the compact layer), referred to as the *diffuse layer* (or *Gouy layer*), is a three-dimensional region of scattered ions, which extends from the OHP into the bulk solution. Such ionic distribution reflects the counterbalance between ordering forces of the electrical field and the disorder caused by a random thermal motion. The equilibrium between these two opposing effects, indicates that the concentration of ionic species at a given distance from the surface, $C(x)$, decays exponentially with the ratio between the electrostatic energy ($zF\Phi$) and the thermal energy (RT), in accordance with the Boltzmann equation):

$$C(x) = C(0)\exp(-zF\Phi)/RT) \tag{1.43}$$

The total charge of the compact and diffuse layers equals (and is opposite in sign) to the net charge on the electrode side. The potential-distance profile across the double-layer region involves two segments, with a linear increase until the OHP and an exponential one within the diffuse layer. Such two-potential drops are displayed in Figure 1.11. Depending on the ionic strength, the thickness of the double layer may extend to more than 10 nm.

The electrical double layer resembles an ordinary (parallel-plate) capacitor. For an ideal capacitor, the charge (q) is directly proportional to the potential difference:

$$q = CE \tag{1.44}$$

where C is the capacitance (in farads, F), specifically, the ratio of the charge stored to the applied potential. The potential–charge relationship for the electrical double layer is

$$q = C_{dl}A(E - E_{pzc}) \tag{1.45}$$

where C_{dl} is the capacitance per unit area and E_{pzc} is the potential of zero charge (i.e., where the sign of the electrode charge reverses and no net charge exists in the double layer). The C_{dl} values are usually in the range of 10–40 μF/cm^2.

The capacitance of the double layer consists of a combination of the capacitance of the compact layer in series with that of the diffuse layer. As is common for two capacitors in series, the total capacitance is given by

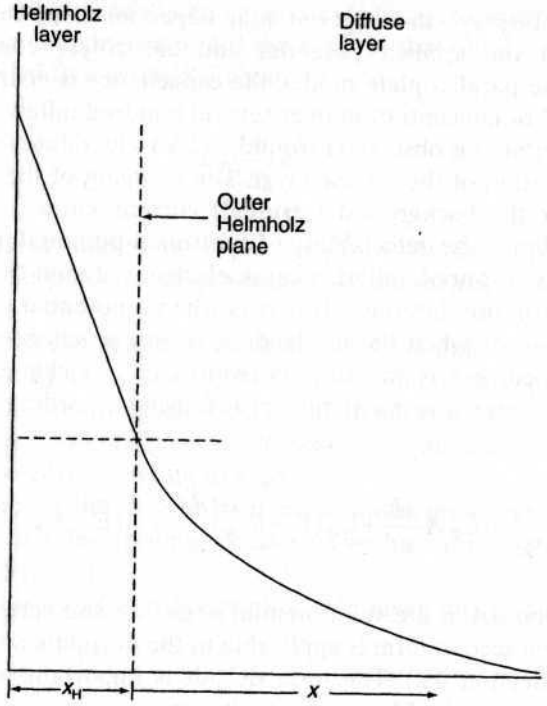

Figure 1.11 Variation of the potential across the electrical double layer.

$$1/C = 1/C_H + 1/C_G \tag{1.46}$$

where C_H and C_G represent that capacitances of the compact and diffuse layers, respectively. The smaller of these capacitances determines the observed behavior. By analogy to a parallel-plate (ideal) capacitor, C_H is given by

$$C_H = -\varepsilon/4\pi d \tag{1.47}$$

where d is the distance between the plates and ε is the dielectric constant. (ε = 78 for water at room temperature.) Accordingly, C_H increases with decreasing separation between the electrode surface and the counterionic layer, as well as with increasing the dielectric constant in the intervening medium. The value of C_G is strongly affected by the electrolyte concentration; the compact layer is largely independent of the concentration. For example, at sufficiently high electrolyte concentration, most of the charge is confined near the Helmholz plane, and little is scattered diffusely into the solution (i.e., the diffuse double layer becomes sufficiently small). Under these conditions, $1/C_H \gg 1/C_G$, $1/C \simeq 1/C_H$, or $C \simeq C_H$. In contrast, for dilute solutions, C_G is very small (compared to C_H) and $C \simeq C_G$.

Figure 1.12 displays the experimental dependence of the double-layer capacitance on the applied potential and electrolyte concentration. As expected for the parallel-plate model, the capacitance is nearly independent of the potential or concentration over several hundred millivolts. Yet, a sharp dip in the capacitance is observed (around –0.5 V) with dilute solutions, reflecting the contribution of the diffuse layer. The charging of the double layer is responsible for the background (residual) current known as the *charging current*, which limits the detectability of controlled-potential techniques. Such a charging process is nonfaradaic because electrons are not transferred across the electrode–solution interface. It occurs when a potential is applied across the double layer, or when the electrode area or capacitances are changing. Note that the current is the time derivative of the charge. Hence, when such processes occur, a residual current is flowing according to the differential equation

$$i = \frac{dq}{dt} = C_{dl}A\frac{dE}{dt} + C_{dl}(E - E_{pzc})\frac{dA}{dt} + A(E - E_{pzc})\frac{dC_{dl}}{dt} \qquad (1.48)$$

where dE/dt and dA/dt are the potential scan rate and rate of area change, respectively. The second term is applicable to the dropping mercury electrode (discussed in Section 4.2). The term dC_{dl}/dt is important when adsorption processes change the double-layer capacitance.

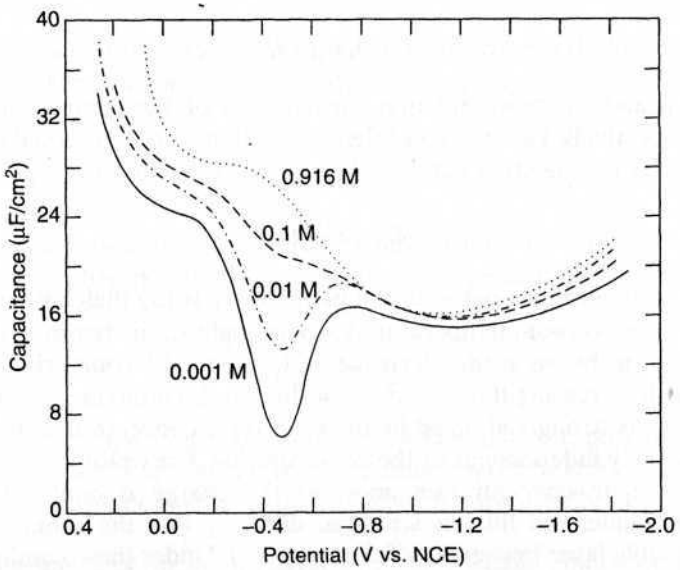

Figure 1.12 Double-layer capacitance of a mercury drop electrode in NaF solutions of different concentrations. (Reproduced with permission from Ref. 5.)

Alternately, for potential-step experiments (e.g., chronoamperometry; see Section 3.1), the charging current is the same as that obtained when a potential step is applied to a series *RC* circuit:

$$i_c = \frac{E}{R_S}e^{-t/RC_{dl}} \qquad (1.49)$$

Thus, the current decreases exponentially with time. Here, E is the magnitude of the potential step, while R_s is the (uncompensated) solution resistance.

Equation (1.48) can be used for calculating the double-layer capacitance of solid electrodes. By recording linear scan voltammograms at different scan rates (using the supporting electrolyte solution), and plotting the charging current (at a given potential) versus the scan rate, one would obtain a straight line, with a slope corresponding to $C_{dl}A$.

Measurements of the double-layer capacitance provide valuable insights into adsorption and desorption processes, as well as into the structure of film-modified electrodes (6).

Further discussion of the electrical double layer can be found in several reviews (5,7–11).

1.4 ELECTROCAPILLARY EFFECT

Electrocapillary is the study of the interfacial tension as a function of the electrode potential. Such a study can shed useful light on the structure and properties of the electrical double layer. The influence of the electrode–solution potential difference on the surface tension (γ) is particularly pronounced at nonrigid electrodes (such as the dropping mercury one, discussed in Section 4.5). A plot of the surface tension versus the potential (like the ones shown in Fig. 1.13) is called an *electrocapillary curve*.

The excess charge on the electrode can be obtained from the slope of the electrocapillary curve (at any potential), by the Lippman equation:

$$\left(\frac{\partial\gamma}{\partial E}\right)_{\text{const.pressure}} = q \qquad (1.50)$$

The more highly charged the interface becomes, the more the charges repel each other, thereby decreasing the cohesive forces and lowering the surface tension. The second differential of the electrocapillary plot gives directly the differential capacitance of the double layer:

$$\frac{\partial^2\gamma}{\partial E^2} = -C_{dl} \qquad (1.51)$$

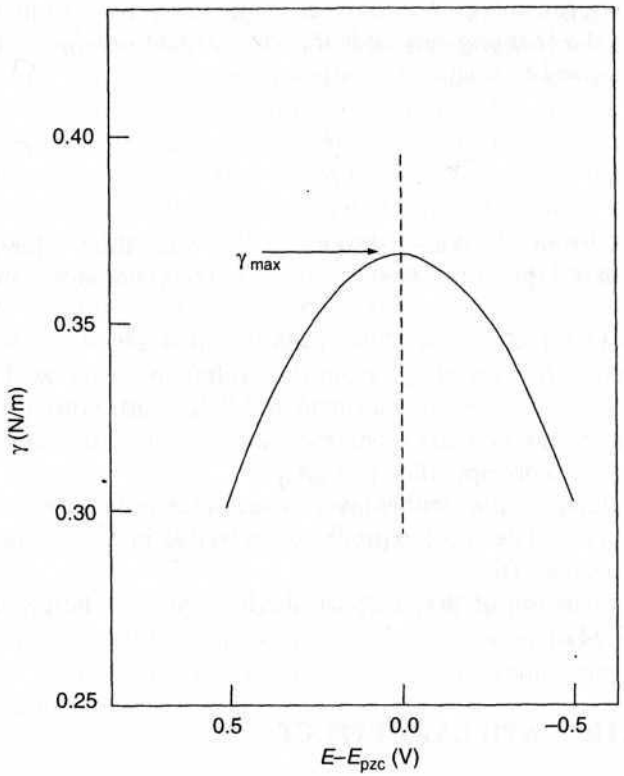

Figure 1.13 Electrocapillary curve of surface tension (γ) versus the potential.

Hence, the differential capacitance represents the slope of the plot of q versus E.

An important point of the electrocapillary curve is its maximum. Such maximum value of γ, obtained when $q = 0$, corresponds to the potential of zero charge (E_{pzc}). The surface tension is a maximum because on the uncharged surface there is no repulsion between like charges. The charge on the electrode changes its sign after passing the potential through the E_{pzc}. Experimental electrocapillary curves have a nearly parabolic shape around the E_{pzc}. Such a parabolic shape corresponds to a linear change of the charge with the potential. The deviation from a parabolic shape depends on the solution composition, particularly on the nature of the anions present in the electrolyte. In particular, specific interaction of various anions (e.g., halides) with the mercury surface, occurring at positive potentials, causes deviations from the parabolic behavior (with shifts of E_{pzc} to more cathodic potentials). As shown in Figure 1.14, the change in surface tension and the negative shift in E_{pzc} increase in the following order: $I^- > Br^- > CNS^- > NO_3^- > OH^-$. (These changes are expected from the strength of the specific adsorption.) Such ions can be specifically

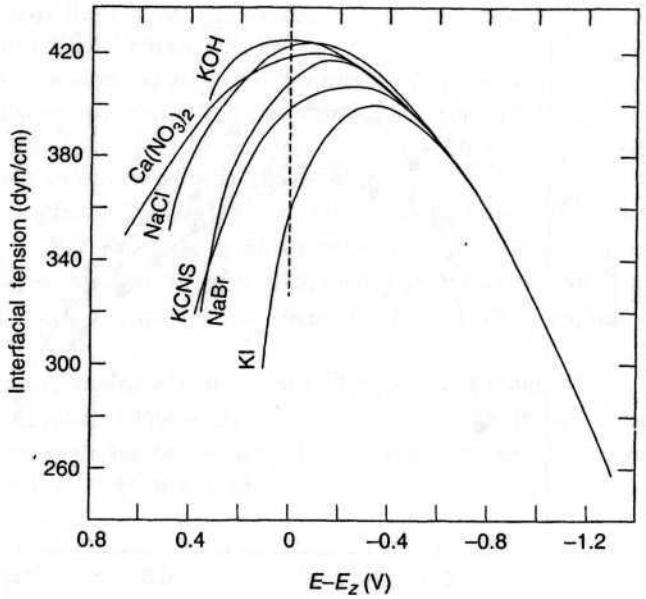

Figure 1.14 Electrocapillary curves for different electrolytes showing the relative strength of specific adsorption. (Reproduced with permission from Ref. 7.)

adsorbed because they are not solvated. Inorganic cations, in contrast, are less specifically adsorbed (because they are usually hydrated). Similarly, blockage of the surface by a neutral adsorbate often causes depressions in the surface tension in the vicinity of the E_{pzc} (Fig. 1.15). Note the reduced dependence of γ on the potential around this potential. At more positive or negative potentials, such adsorbates are displaced from the surface by oriented water molecules.

1.5 SUPPLEMENTARY READING

Several international journals bring together papers and reviews covering innovations and trends in the field of electroanalytical chemistry:

Bioelectrochemistry and Bioenergetics
Biosensors and Bioelectronics
Electroanalysis
Electrochemistry Communications
Electrochimica Acta
Journal of Applied Electrochemistry
Journal of Electroanalytical and Interfacial Electrochemistry

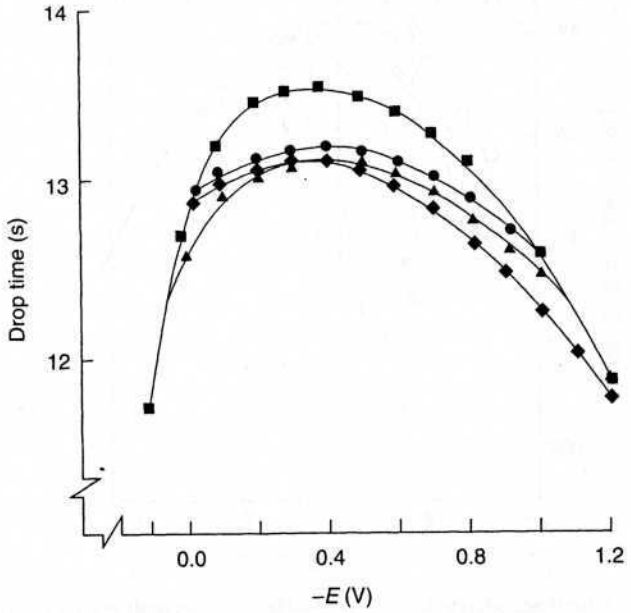

Figure 1.15 Electrocapillary curves of background (■), ethynylestradiol (●), β-estradion (△), and morgestrel (◆). (Reproduced with permission from Ref. 12.)

Journal of the Electrochemical Society
Langmuir
Sensors and Actuators

Useful information can be found in many prominent journals that cater to all branches of analytical chemistry, including *The Analyst*, *Analytica Chimica Acta*, *Analytical Chemistry*, *Talanta*, *Analytical Letters*, and *Analytical and Bioanalytical Chemistry*. Biennial reviews published in the June issue of *Analytical Chemistry* offer comprehensive summaries of fundamental and practical research work.

Many textbooks and reference works dealing with various aspects of electroanalytical chemistry have been published since the 1960s. Some of these are listed below as suggestions for additional reading, in alphabetic order:

Albery, W. J., *Electrode Kinetics*, Clarendon Press, Oxford, UK, 1975.

Bard, A. J.; Faulkner, L., *Electrochemical Methods*, 2nd ed., Wiley, New York, 2000.

Bond, A. M., *Modern Polarographic Methods in Analytical Chemistry*, Marcel Dekker, New York, 1980.

Bockris, J. M.; Reddy, A., *Modern Electrochemistry*, Vols. 1, 2, Plenum Press, New York, 1970.

Brett, C.; Oliveira Brett, A. M., *Electrochemistry: Principles, Methods and Applications*, Oxford Univ. Press, Oxford, UK, 1993.

Diamond, D., *Chemical and Biological Sensors*, Wiley, New York, 1998.

Gileadi, E., *Electrode Kinetics*, VCH Publishers, New York, 1993.

Kissinger, P.; Heineman, W., *Laboratory Techniques in Electroanalytical Chemisry*, 2nd ed., Marcel Dekker, New York, 1996.

Janata, J., *Principles of Chemical Sensors*, Plenum Press, New York, 1989.

Koryta, J.; Dvorak, J., *Principles of Electrochemistry*, Wiley, Chichester, UK, 1987.

Rieger, P., *Electrochemistry*, Prentice-Hall, Englewood Cliffs, NJ, 1987.

Sawyer, D.; Roberts, J., *Experimental Electrochemistry for Chemists*, Wiley, New York, 1974.

Smyth, M.; Vos, J., *Analytical Voltammetry*, Elsevier, Amsterdam, 1992.

Turner, A. P.; Karube, I.; Wilson, G., *Biosensors*, Oxford Univ. Press, Oxford, UK, 1987.

Wang, J., *Electroanalytical Techniques in Clinical Chemistry and Laboratory Medicine*, VCH Publishers, New York, 1988.

PROBLEMS

1.1 Describe and draw the concentration profile or gradient near the electrode surface during a linear scan voltammetric experiment in a *stirred* solution. (Use five or six potentials on both sides of $E°$.) Show also the resulting voltammogram, along with points for each concentration gradient (in a manner analogous to Fig. 1.4).

1.2 Describe and draw the structure of the electrical double layer (with its several distinct parts).

1.3 Use the activated complex theory for explaining how the applied potential affects the rate constant of an electron transfer reaction. Use or draw free-energy curves and use proper equations for your explanation.

1.4 Use equations to demonstrate how an increase in the stirring rate will affect the mass-transport-controlled limiting current.

1.5 Derive the Nernst equation from the Butler–Volmer equation.

1.6 Explain clearly why polyanionic DNA molecules adsorb onto electrode surfaces at potentials more positive than E_{pzc}, and suggest a protocol for desorbing them back to the solution.

1.7 Which experimental conditions assure that the movement of the electroactive species is limited by diffusion? How do these conditions suppress the migration and convection effects?

1.8 Explain clearly the reason for the peaked response of linear sweep voltammetric experiments involving a planar macrodisk electrode and a quiescent solution.

1.9 The net current flowing at the equilibrium potential is zero, yet this is a dynamic situation with equal opposing cathodic and anodic current components (whose absolute value is i_0). Suggest an experimental route for estimating the value of i_0.

1.10 Explain clearly why only a fraction of the energy shift (associated with a potential shift) is used for increasing the activation energy barrier.

REFERENCES

1. Maloy, J. R., *J. Chem. Educ.* **60**, 285 (1983).
2. Smith, M. G., *Laplace Transform Theory*, Van Nostrand, London, 1966.
3. Compton, R. G.; Eklund, J.; Marken, F., *Electroanalysis* **9**, 509 (1997).
4. Grundler, P.; Kirbs, A., *Electroanalysis* **11**, 223 (1999).
5. Grahame, D., *Chem. Rev.* **41**, 441 (1947).
6. Swietlow, A.; Skoog, M.; Johansson, G., *Electroanalysis* **4**, 921 (1992).
7. Grahame, D. C., *Ann. Rev. Phys. Chem.* **6**, 337 (1955).
8. Mohilner, D., *J. Electroanal. Chem.* **1**, 241 (1966).
9. Bockris, O'M.; Devanathan, M. A.; Muller, K., *Proc. Roy. Soc. Lond.* **55**, A274 (1963).
10. Parsons, R., *J. Electrochem. Soc.* **127**, 176C (1980).
11. Mark, H. B., *Analyst* **115**, 667 (1990).
12. Bond, A. M.; Heritage, I.; Briggs, M., *Langmuir* **1**, 110 (1985).

2

STUDY OF ELECTRODE REACTIONS AND INTERFACIAL PROPERTIES

2.1 CYCLIC VOLTAMMETRY

Cyclic voltammetry is the most widely used technique for acquiring qualitative information about electrochemical reactions. The power of cyclic voltammetry results from its ability to rapidly provide considerable information on the thermodynamics of redox processes and the kinetics of heterogeneous electron transfer reactions and on coupled chemical reactions or adsorption processes. Cyclic voltammetry is often the first experiment performed in an electroanalytical study. In particular, it offers a rapid location of redox potentials of the electroactive species, and convenient evaluation of the effect of media on the redox process.

Cyclic voltammetry consists of scanning linearly the potential of a stationary working electrode (in an unstirred solution), using a triangular potential waveform (Fig. 2.1). Depending on the information sought, single or multiple cycles can be used. During the potential sweep, the potentiostat measures the current resulting from the applied potential. The resulting current–potential plot is termed a *cyclic voltammogram*. The cyclic voltammogram is a complicated, time-dependent function of a large number of physical and chemical parameters.

Figure 2.2 illustrates the expected response of a reversible redox couple during a single potential cycle. It is assumed that only the oxidized form O is present initially. Thus, a negative-going potential scan is chosen for the first half-cycle, starting from a value where no reduction occurs. As the applied

Analytical Electrochemistry, Third Edition, by Joseph Wang
Copyright © 2006 John Wiley & Sons, Inc.